

## SUPPORTING INFORMATION

### THE INTERPLAY BETWEEN NUCLEATION AND PATTERNING DURING SHEAR-INDUCED CRYSTALLIZATION FROM SOLUTION IN A PARALLEL PLATE GEOMETRY

Cedric Devos,<sup>a</sup> Anja Vananroye,<sup>a</sup> Ruth Cardinaels,<sup>ab</sup> Christos Xiouras,<sup>c</sup> Tom Van Gerven,<sup>a</sup> and  
Simon Kuhn\*<sup>a</sup>

<sup>a</sup> KU LEUVEN, DEPARTMENT OF CHEMICAL ENGINEERING, CELESTIJNENLAAN 200F, 3001  
LEUVEN, BELGIUM

<sup>b</sup> TU EINDHOVEN, DEPARTMENT OF MECHANICAL ENGINEERING, 5600 MB EINDHOVEN, THE  
NETHERLANDS

<sup>c</sup> JANSSEN PHARMACEUTICAL COMPANIES OF JOHNSON & JOHNSON, JANSSEN RESEARCH AND  
DEVELOPMENT, CRYSTALLIZATION TECHNOLOGY UNIT (CTU), 2340 BEERSE, BELGIUM

\* SIMON.KUHN@KULEUVEN.BE

### Contents

1	The effect of centrifugal forces	2
2	Crystal detection	2
3	Nucleation data	4
4	Crystal size	14
5	Shear stress response curves	15
6	Video files	16

# 1 The effect of centrifugal forces

Centrifugal forces act on the crystals in the solution and push them towards the zones of higher fluid shear. An experiment was performed to study crystal migration towards the edges of the parallel plate due to centrifugal forces. These experiments were performed with 3.0 mL of solution volume and a gap size of 2.00 mm, as the crystals have more freedom to move around in larger solution volumes. Then, the time evolution of the nucleation location was monitored. An example of the result is shown in Figure 1. An overview of different individual measurements is shown in Figure 2. Only for the highest shear rate of 200 1/s we see that the nucleation location is slightly impacted by particle migration, but nucleation times at this shear rate were also shorter than the time it takes for crystals to move. Hence, it can be concluded that the centrifugal forces did not affect the experiments shown in the manuscript.

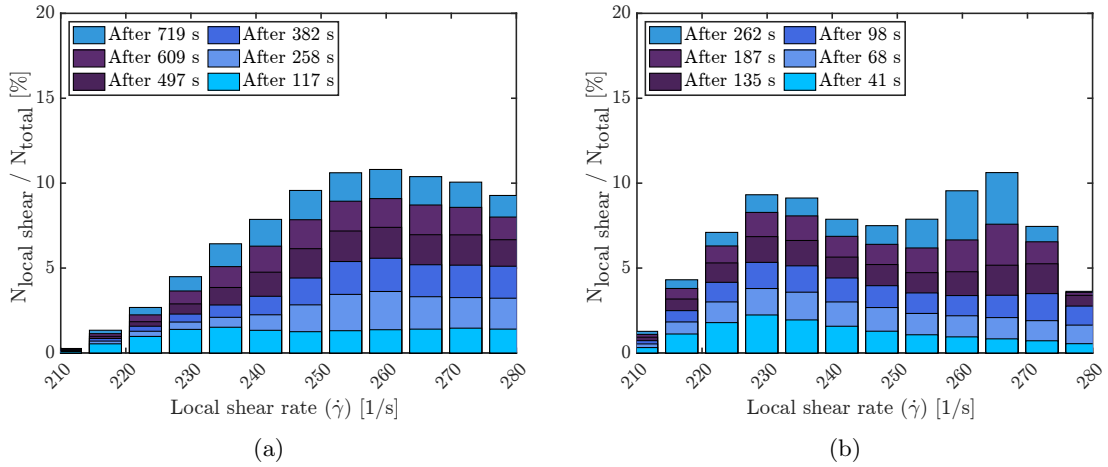


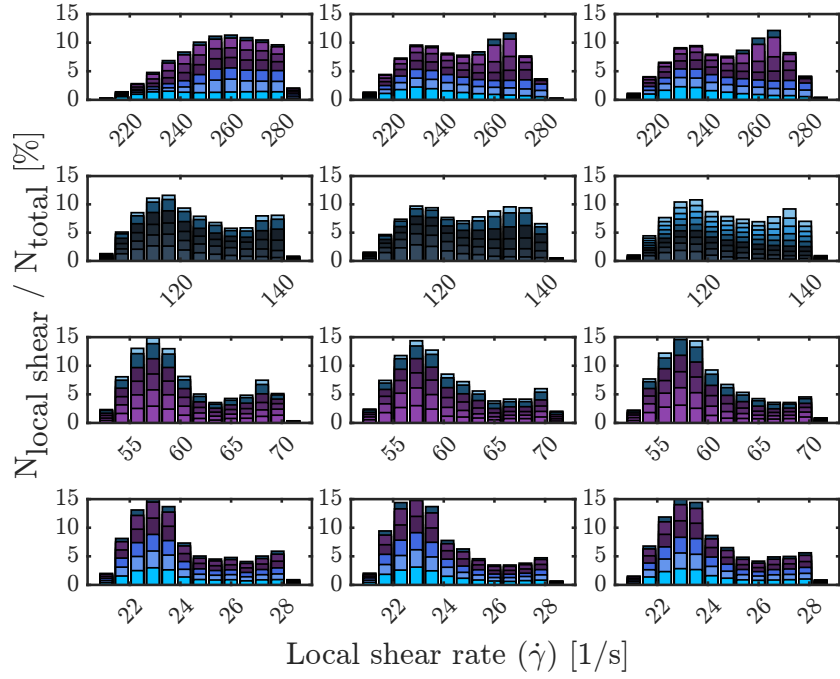
Figure 1: Time evolution of the ratio of the number of crystals in a discretized local shear rate ( $\dot{\gamma}$ ) interval (defined as  $N_{\text{local shear}}$ ) and the total number of crystals (for a gap of 2.00 mm). Zones between  $2/3 \cdot R_{\text{max}}$  and  $R_{\text{max}}$  are shown. Both curves are for a global shear rate ( $\bar{\dot{\gamma}}$ ) of 200 1/s.

# 2 Crystal detection

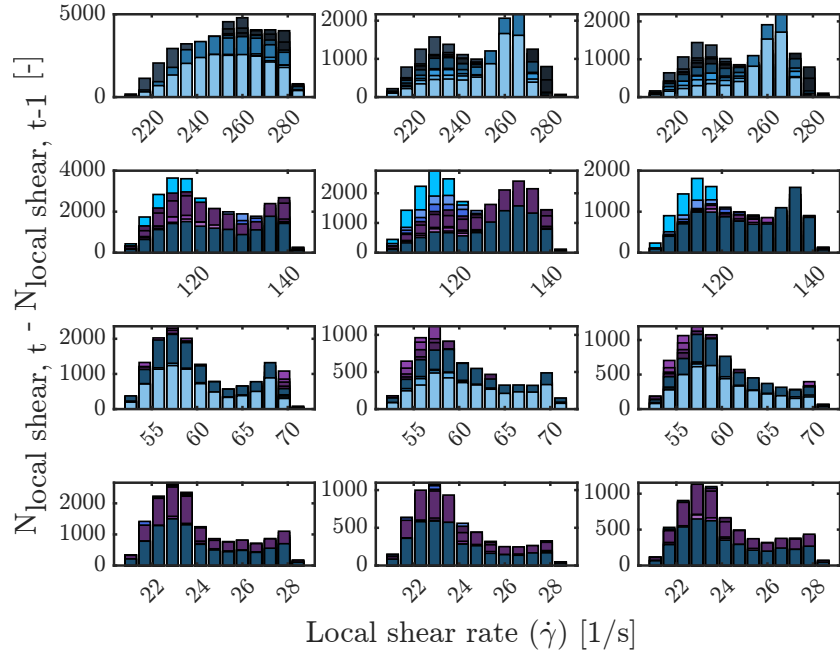
The onset of crystallization is detected using a high-speed camera (as explained in Section 2 of the manuscript). The solution flowing between  $2/3 \cdot R_{\text{max}}$  and  $R_{\text{max}}$  is monitored continuously throughout an experiment. The detection zone is shown in purple in Figure 3. The number of crystals detected by the particle detection software (as explained in Section 2 of the manuscript) is counted as function of time ( $N(t)$ ).

Figure 4 depicts the detection of crystals adhered to the top plate. As the top plate rotates, the crystals move along with it. The particle detection software identifies and counts the crystals that pass through the detection zone. However, if a crystal passes through multiple times, it is double-counted. The detection zone is then also divided into several intervals, and the total number of crystals passing through each interval is tallied.

Figure 5 shows images before and after processing with the particle detection software, as discussed in Section 2 of the manuscript. The images clearly demonstrate that all the crystals, except



(a)



(b)

Figure 2: (a) Time evolution of the ratio of the number of crystals in a discretized local shear rate ( $\dot{\gamma}$ ) interval (defined as  $N_{\text{local shear}}$ ) and the total number of crystals (for a gap of 2.00 mm). (b) Time evolution of the difference between the number of crystals in a discretized local shear rate ( $\dot{\gamma}$ ) interval (defined as  $N_{\text{local shear}}$ ) at time  $t$  and at time  $t - 1$  (for a gap of 2.00 mm). Zones between  $2/3 \cdot R_{\text{max}}$  and  $R_{\text{max}}$  are shown in (a) and (b). Every subplot is an experiment. Different colors represent different times (discretized linearly from the start of the experiment until the end).

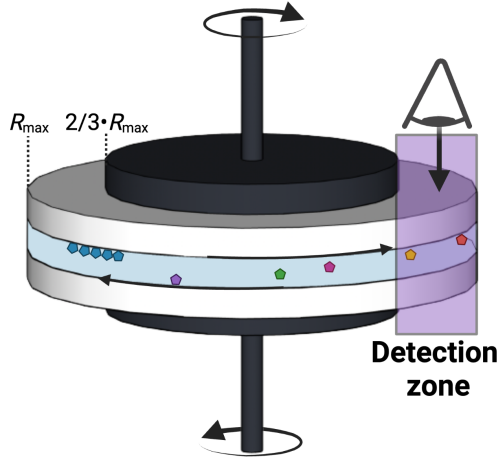


Figure 3: Illustration showcasing crystal detection in the parallel plate geometry, highlighting the detection zone in purple. Crystals are shown as small pentagons in different colors. The solution flowing between  $2/3 \cdot R_{\max}$  and  $R_{\max}$  is imaged.

for those located at the frame's edges, are accurately detected through the software.

### 3 Nucleation data

In this section additional nucleation data is shown. The ratio of the number of crystals in a certain discretized local shear rate interval and the total number of detected crystals for a gap of 2.00 mm is shown in Figure 6. The experimental cumulative nucleation probabilities ( $P_{\text{exp}}(t)$ ) for a gap size of 0.50 mm and 2.00 mm are shown in Figure 8. The total number of detected crystals as a function of time are shown in Figure 10, for a gap of 0.50 and 2.00 mm, respectively. Figure 12 and 14 show the number of crystals discretized in local shear rate intervals for gap sizes of 0.50 and 2.00 mm, respectively, for all experiments.

The experimental cumulative nucleation probability ( $P(t)$ ) is the probability that at least 1 nucleus has formed in a time interval  $t$ <sup>1</sup> and can be calculated using equation 1, with  $M_{\geq 1}$  the number of experiments in which crystals are detected at time  $t$ , and  $M$  the total number of experiments.

$$P_{\geq 1, \text{exp}}(t) = \frac{M_{\geq 1}(t)}{M} \quad (1)$$

In Figure 7 the number of crystals detected in a local shear rate interval ( $N_{\text{local shear}}$ ) is normalized by the volume of that local shear rate interval ( $V_{\text{local shear}}$ ). This volume is calculated using equation 2, with  $h$  the gap size, and  $r$  the radius.

$$V_{\text{local shear}} = \int_{r_{\text{start interval}}}^{r_{\text{end interval}}} 2\pi hr \, dr \quad (2)$$

Figure 9 presents the average time elapsed before nucleation is observed for different global shear rates. This figure displays identical data to that presented in Figure 2 of the manuscript.

<sup>1</sup>S. Jiang and J. H. Ter Horst, Cryst. Growth Des., 2011, 11, 256–261.

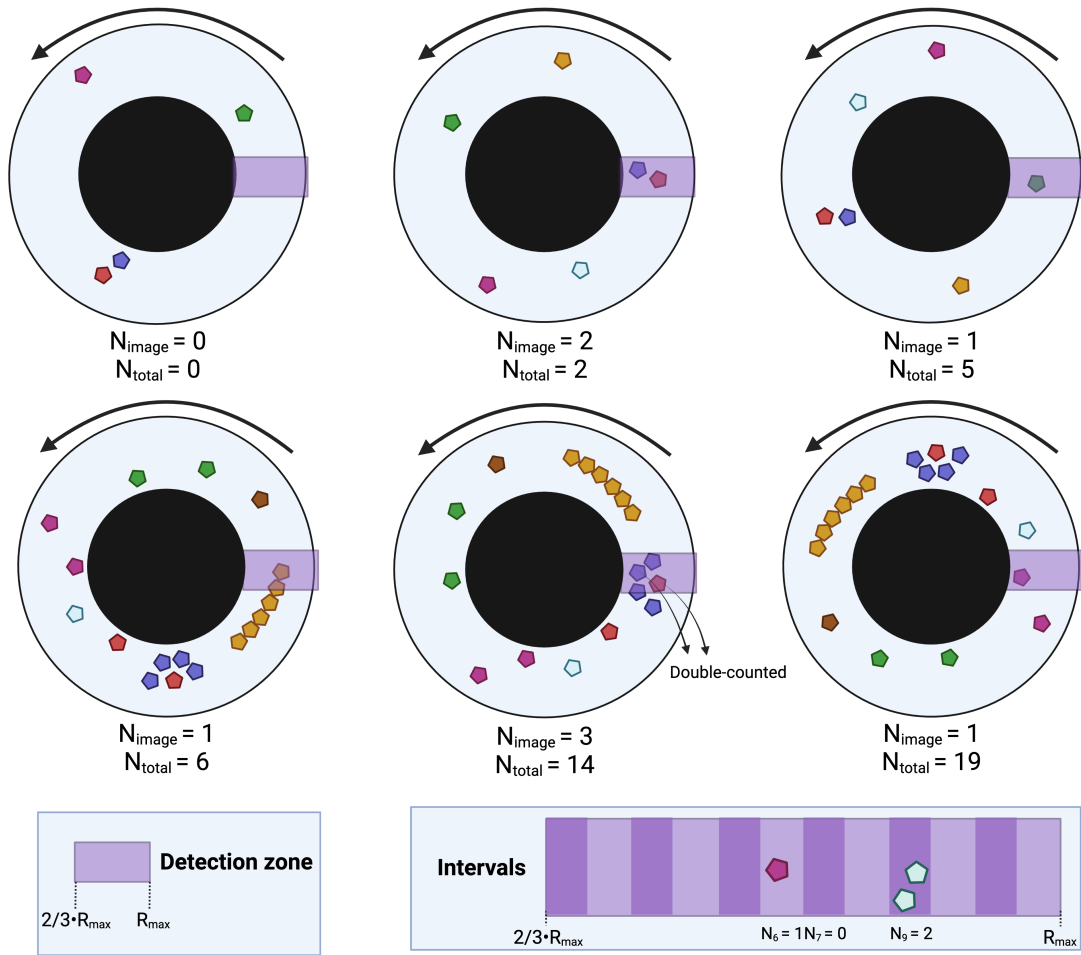


Figure 4: Illustration showcasing crystal detection in the parallel plate geometry for crystals stuck on the top plate, highlighting the detection zone in purple. The top plate is viewed from a top view perspective. Crystals are shown as small pentagons in different colors. The total cumulative number of detected crystals ( $N_{\text{total}}$ ) and the number of detected crystals per frame ( $N_{\text{image}}$ ) are mentioned. The bottom right figure illustrates how the detection zone is discretized in local shear rate intervals.

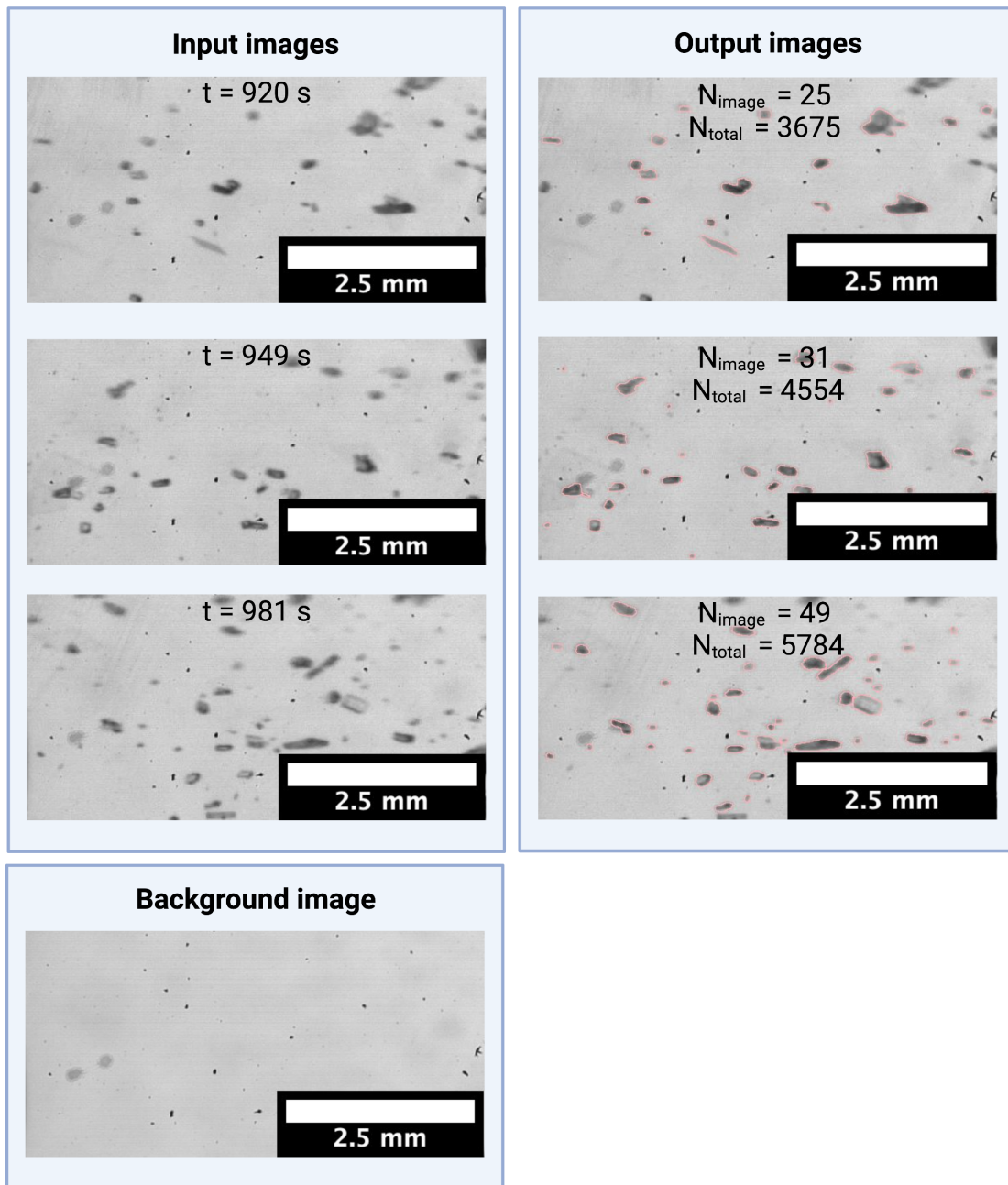


Figure 5: An illustration showcasing frames before and after undergoing processing with the particle detection software. The recorded image includes the experimental time ( $t$ ). The number of crystals detected in each frame ( $N_{\text{image}}$ ) and the cumulative count of crystals detected thus far ( $N_{\text{total}}$ ) are indicated. The image displayed in the bottom left corner represents the background. Every crystal that is counted is outlined in red.

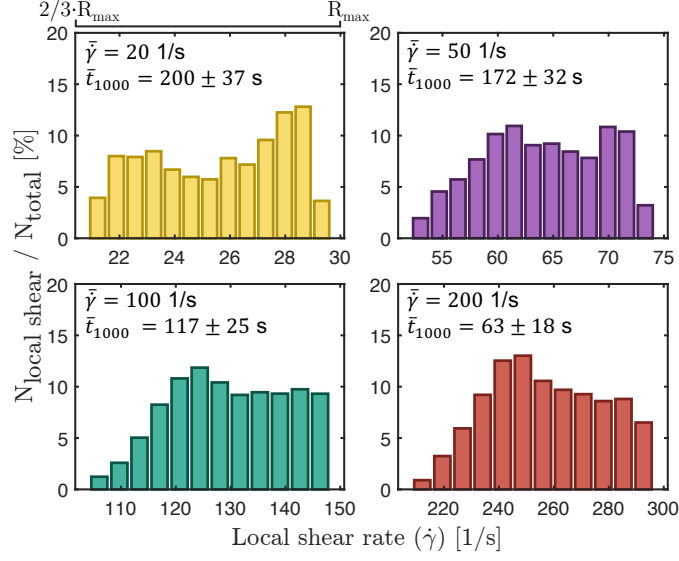


Figure 6: Ratio of the number of crystals in a discretized local shear rate ( $\dot{\gamma}$ ) interval (defined as  $N_{\text{local shear}}$ ) and the total number of crystals (for a gap of 2.00 mm). Zones between  $2/3 \cdot R_{\text{max}}$  and  $R_{\text{max}}$  are shown. The graphs are calculated based on the first 1000 crystals ( $N_{\text{total}}$ ) that are cumulatively detected. The top left corner of each subplot shows the average time difference between the cumulative detection of the 1000<sup>th</sup> and the 5<sup>th</sup> crystal ( $\bar{t}_{1000}$ ) at the global shear rates ( $\bar{\dot{\gamma}}$ ) of 20, 50, 100, and 200 1/s. Each curve is the mean of 16 individual measurements.

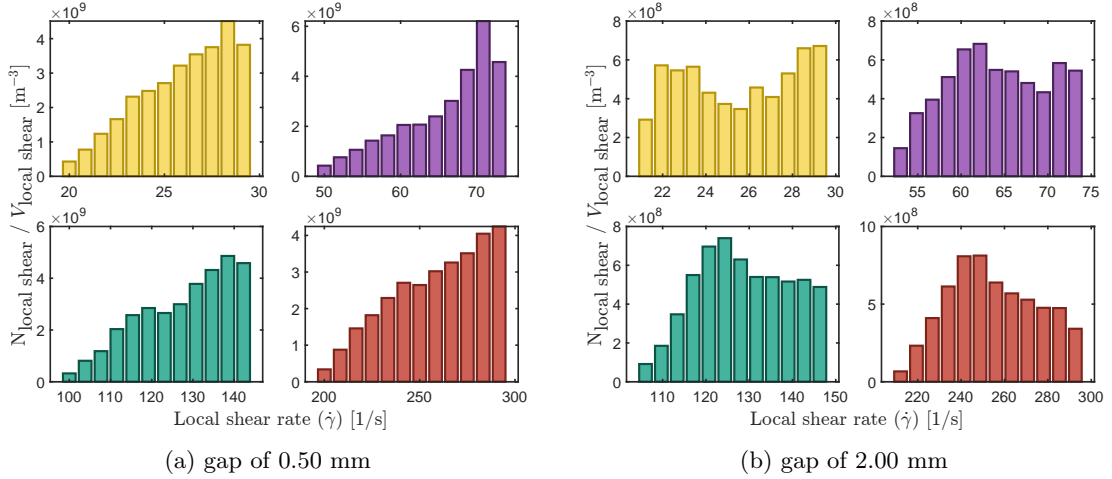


Figure 7: Ratio of the number of crystals in a discretized local shear rate ( $\dot{\gamma}$ ) interval (defined as  $N_{\text{local shear}}$ ) and the volume of that interval. Zones between  $2/3 \cdot R_{\text{max}}$  and  $R_{\text{max}}$  are shown. The graphs are calculated based on the first 1000 crystals ( $N_{\text{total}}$ ) that are cumulatively detected. Each graph represents the mean of several individual measurements.

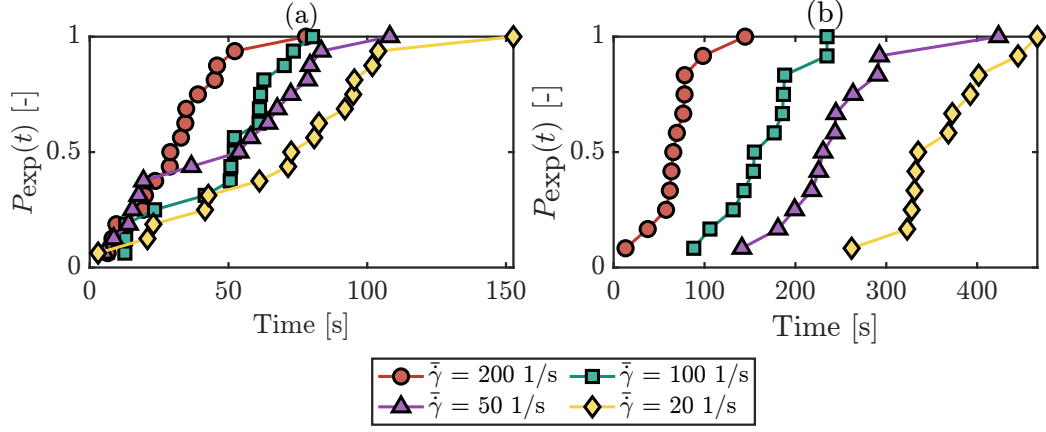


Figure 8: Experimental cumulative nucleation probabilities ( $P_{\text{exp}}(t)$ ) for global shear rates ( $\bar{\gamma}$ ) of 20, 50, 100, and 200 1/s, calculated using equation 1, for (a) a gap of 0.50 mm, and (b) a gap of 2.00 mm.

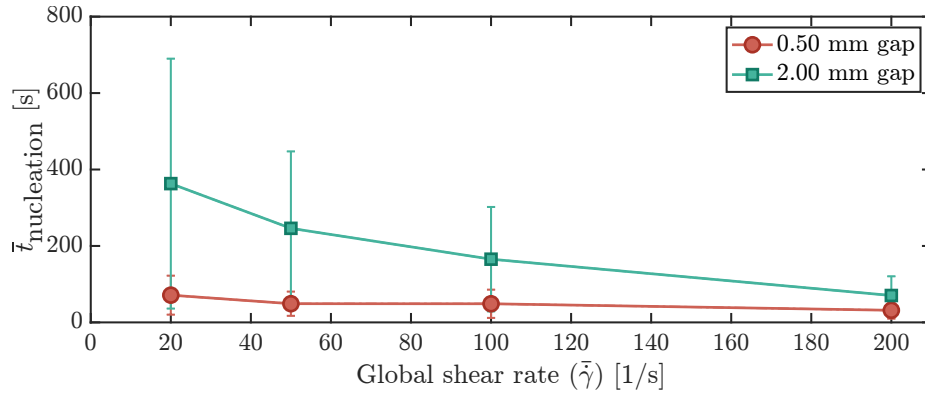


Figure 9: The mean time before nucleation is detected ( $\bar{t}_{\text{nucleation}}$ ) for various global shear rates ( $\bar{\gamma}$ ) for gap sizes of 0.50 mm and 2.00 mm in red and green, respectively.

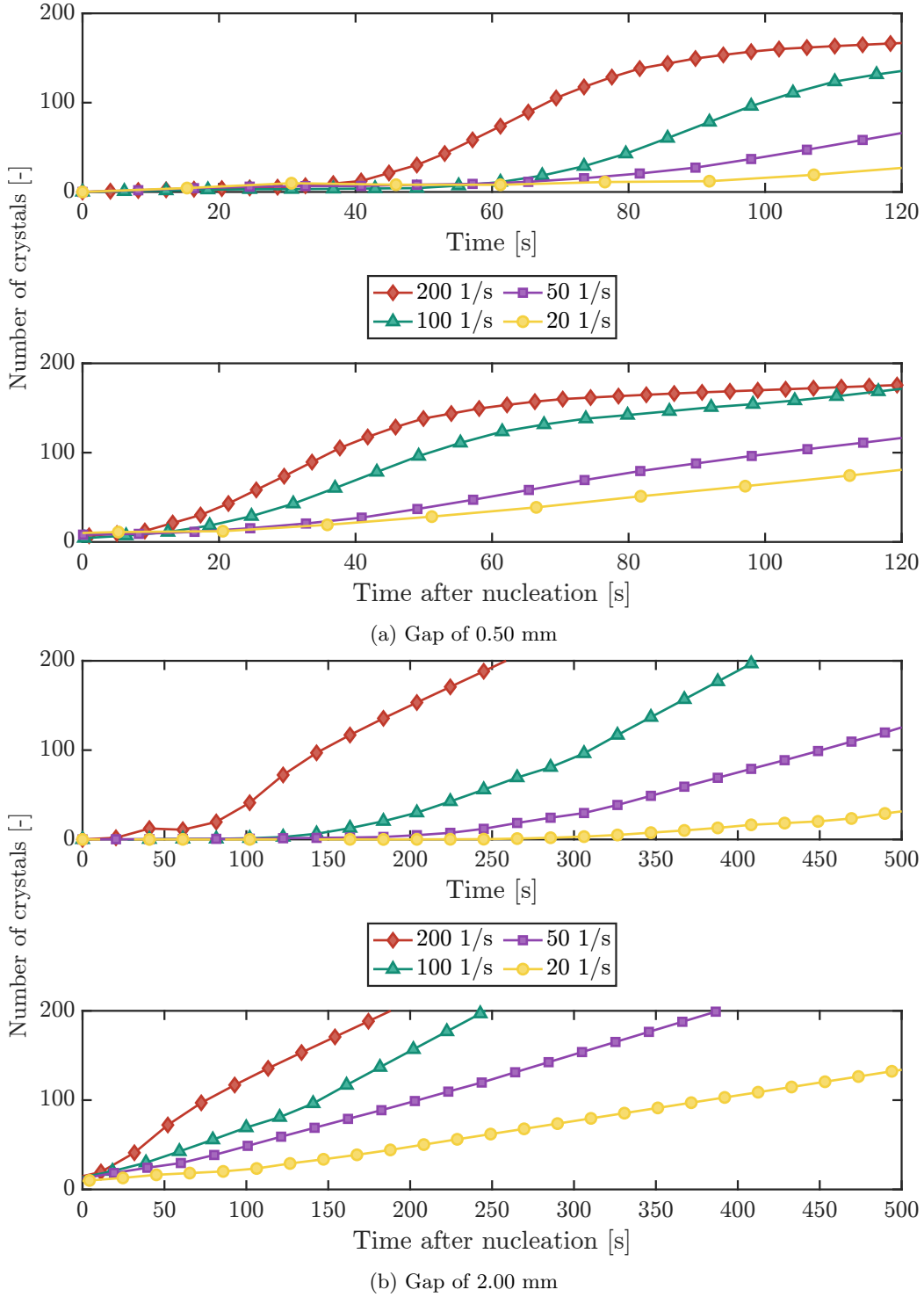
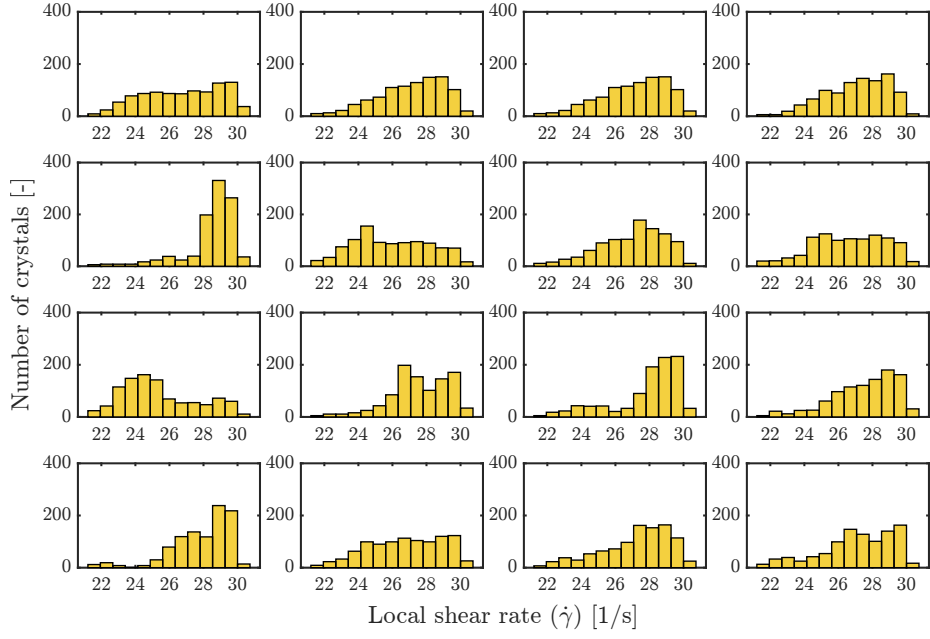
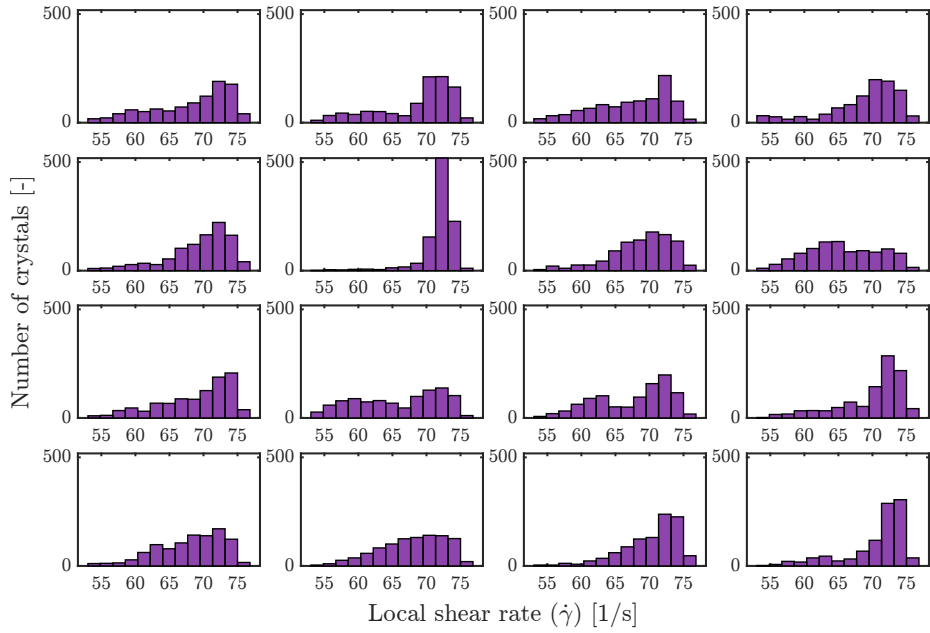


Figure 10: Number of detected crystals ( $N$ ) as a (top graph) function of time from the start of an experiment and (bottom graph) function of the time after nucleation for four global shear rates ( $\dot{\gamma}$ ). The number of crystals ( $N$ ) is defined here as the number of crystals detected in one single frame ( $N_{\text{image}}$ ) from  $2/3 \cdot R_{\text{max}}$  and  $R_{\text{max}}$ . The curves shown here are the mean values of 16 (for a gap of 0.50 mm) and 12 (for a gap of 2.00 mm) individual experiments. The markers are a guide for the eye.

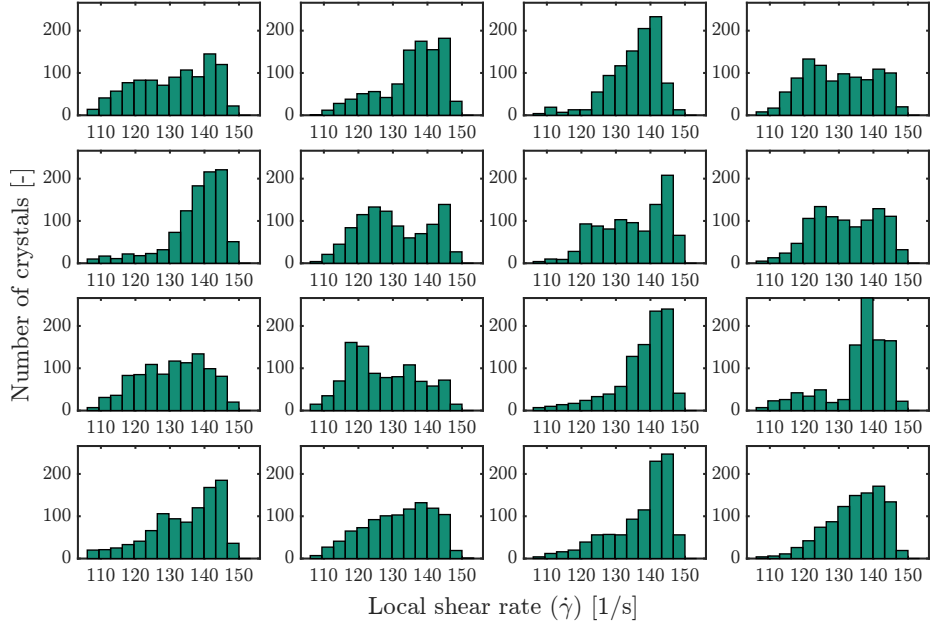


(a)  $\bar{\dot{\gamma}} = 20 \text{ 1/s}$

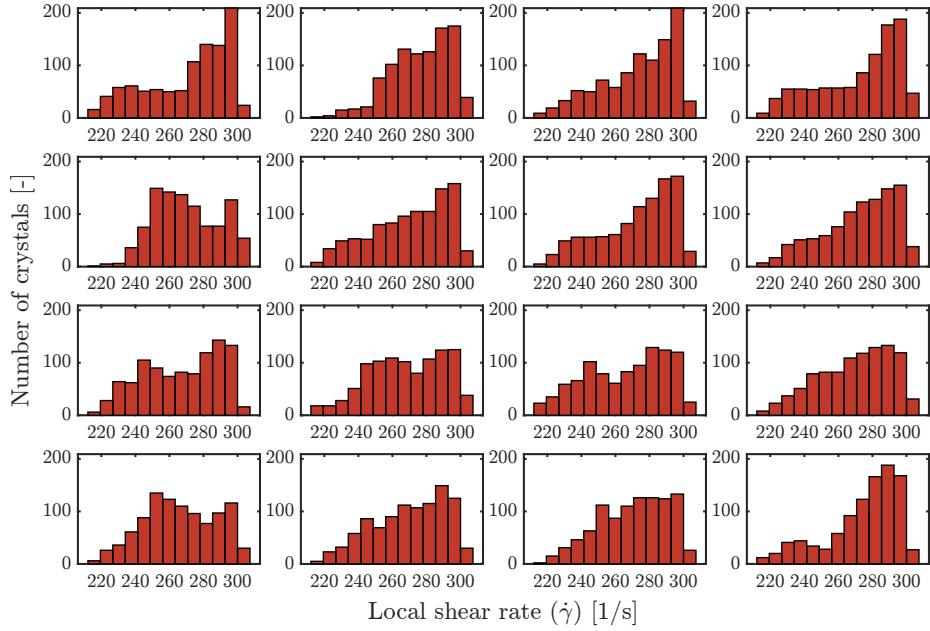


(b)  $\bar{\dot{\gamma}} = 50 \text{ 1/s}$

Figure 11: Number of crystals detected in different discretized local shear rate ( $\dot{\gamma}$ ) intervals (for a gap of 0.50 mm) for a global shear rate ( $\bar{\dot{\gamma}}$ ) of (a)  $20 \text{ s}^{-1}$ , and (b)  $50 \text{ s}^{-1}$ , respectively. Zones between  $2/3 \cdot R_{\text{max}}$  and  $R_{\text{max}}$  are shown. The graphs show the first 1000 crystals ( $N_{\text{total}}$ ) that are cumulatively detected. Every subplot shows an experiment.

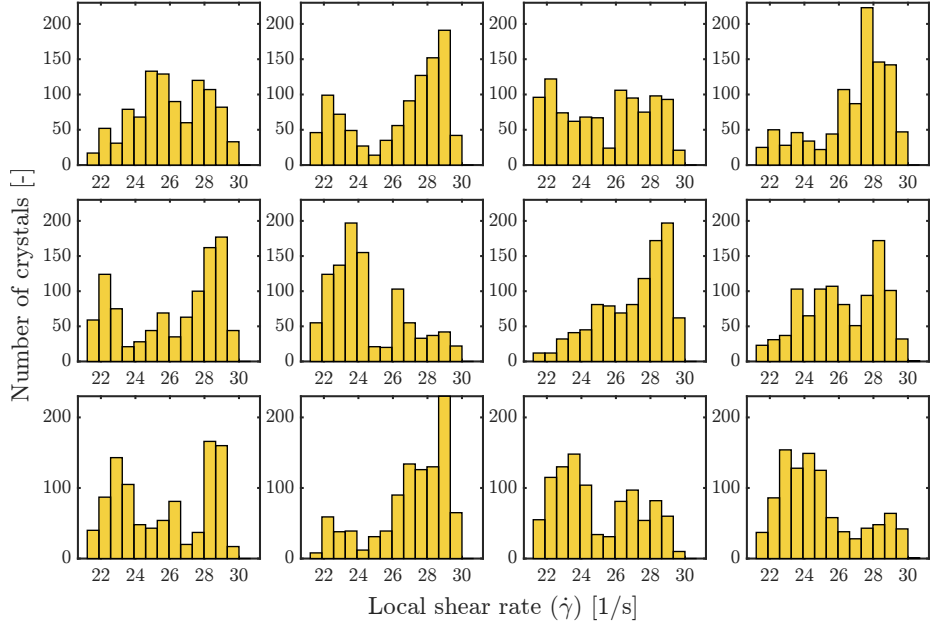


(a)  $\bar{\dot{\gamma}} = 100 \text{ 1/s}$

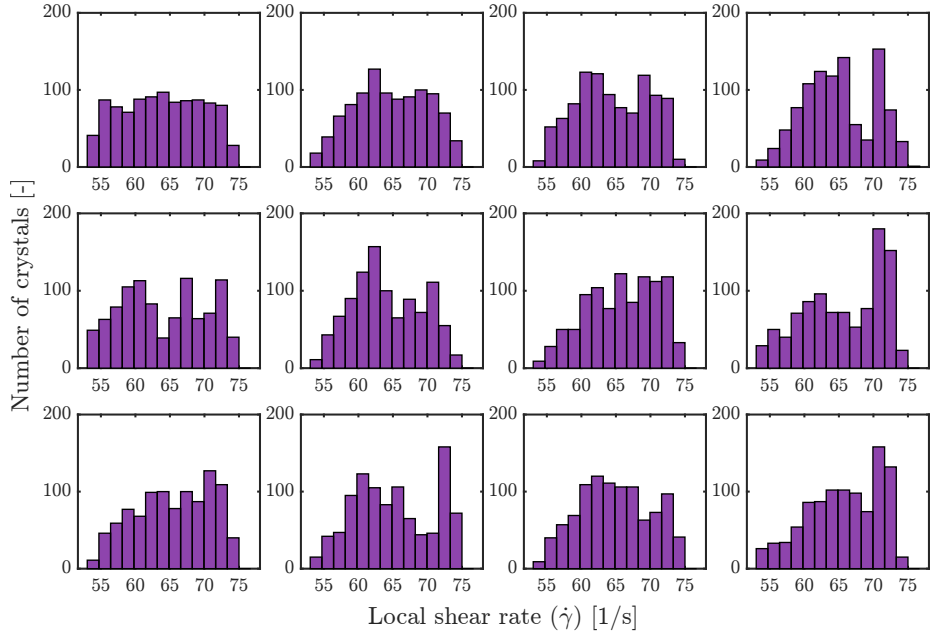


(b)  $\bar{\dot{\gamma}} = 200 \text{ 1/s}$

Figure 12: Number of crystals detected in different discretized local shear rate ( $\dot{\gamma}$ ) intervals (for a gap of 0.50 mm) for a global shear rate ( $\bar{\dot{\gamma}}$ ) of (a)  $100 \text{ s}^{-1}$ , and (b)  $200 \text{ s}^{-1}$ , respectively. Zones between  $2/3 \cdot R_{\text{max}}$  and  $R_{\text{max}}$  are shown. The graphs show the first 1000 crystals ( $N_{\text{total}}$ ) that are cumulatively detected. Every subplot shows an experiment. (cont.)

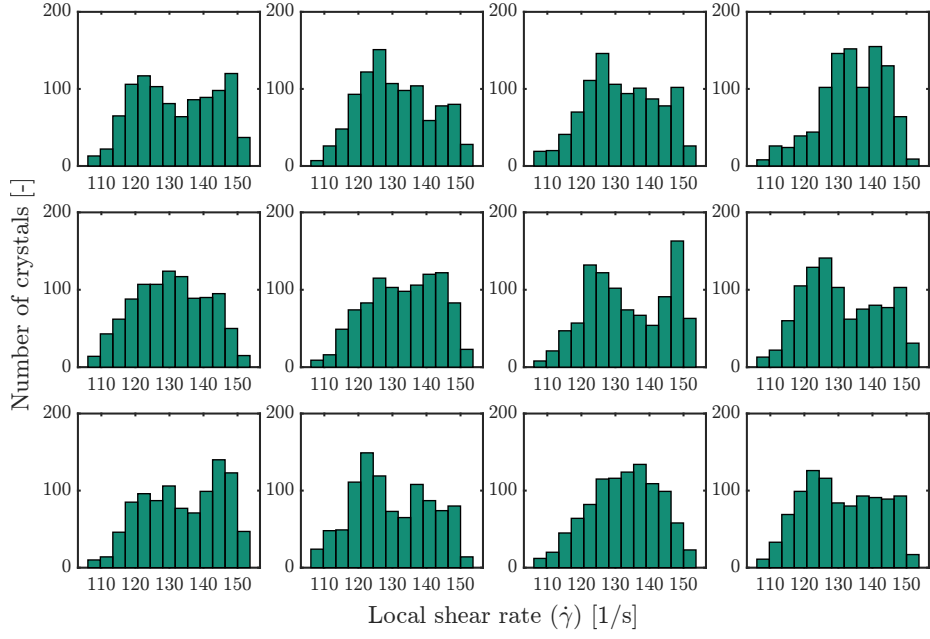


(a)  $\bar{\dot{\gamma}} = 20$  1/s

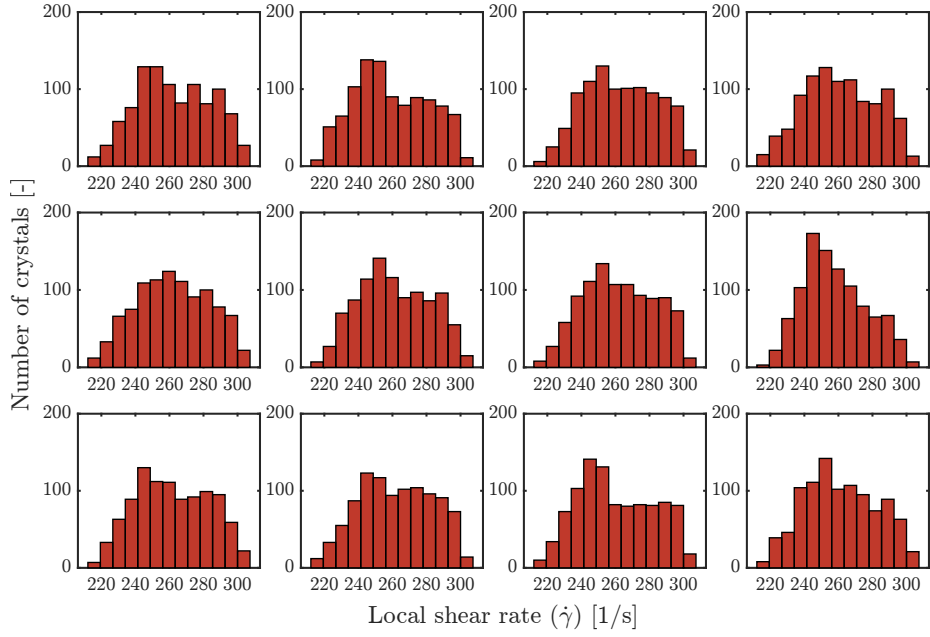


(b)  $\bar{\dot{\gamma}} = 50$  1/s

Figure 13: Number of crystals detected in different discretized local shear rate ( $\dot{\gamma}$ ) intervals (for a gap of 2.00 mm) for a global shear rate ( $\bar{\dot{\gamma}}$ ) of (a)  $20 \text{ s}^{-1}$ , and (b)  $50 \text{ s}^{-1}$ , respectively. Zones between  $2/3 \cdot R_{\max}$  and  $R_{\max}$  are shown. The graphs show the first 1000 crystals ( $N_{\text{total}}$ ) that are cumulatively detected. Every subplot shows an experiment.



(a)  $\bar{\dot{\gamma}} = 100 \text{ 1/s}$



(b)  $\bar{\dot{\gamma}} = 200 \text{ 1/s}$

Figure 14: Number of crystals detected in different discretized local shear rate ( $\dot{\gamma}$ ) intervals (for a gap of 2.00 mm) for a global shear rate ( $\bar{\dot{\gamma}}$ ) of (a)  $100 \text{ s}^{-1}$ , and (b)  $200 \text{ s}^{-1}$ , respectively. Zones between  $2/3 \cdot R_{\max}$  and  $R_{\max}$  are shown. The graphs show the first 1000 crystals ( $N_{\text{total}}$ ) that are cumulatively detected. Every subplot shows an experiment. (cont.)

## 4 Crystal size

The product crystals, for example those shown in Figure 15, exhibit varying sizes depending on the experimental conditions. The span is used as a measure for the spread on the size distribution and can be calculated using equation 3 with  $D_{n,90}$ ,  $D_{n,10}$ , and  $D_{n,50}$  the percentiles of the distribution. The crystals on the top plate, including those in the strings, have a span of 1.35, whereas the crystals on the bottom plate, either after nucleation directly on the surface or after sedimentation from the bulk, have a span of 1.99.

$$\text{Span} = \frac{D_{n,90} - D_{n,10}}{D_{n,50}} \quad (3)$$

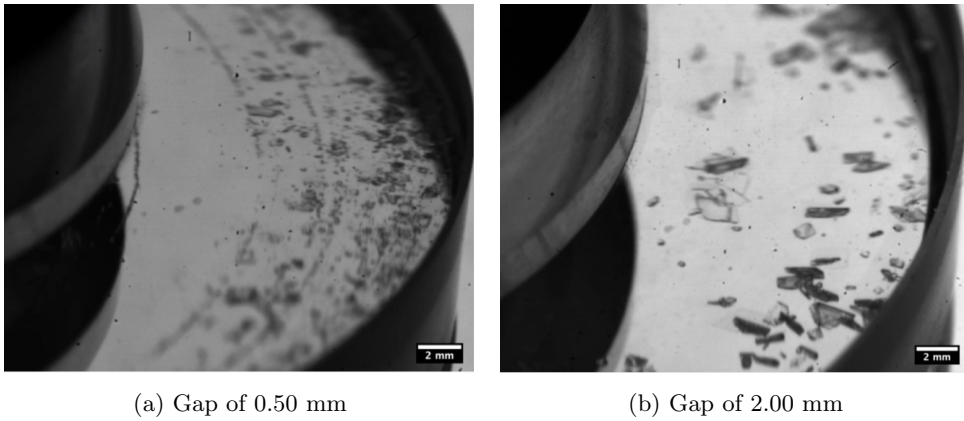


Figure 15: Images of the product crystals in the parallel plate geometry, for an experiment conducted with a global shear rate ( $\dot{\gamma}$ ) of 20 1/s. More crystals are detected at higher local shear rates (right side of each image).

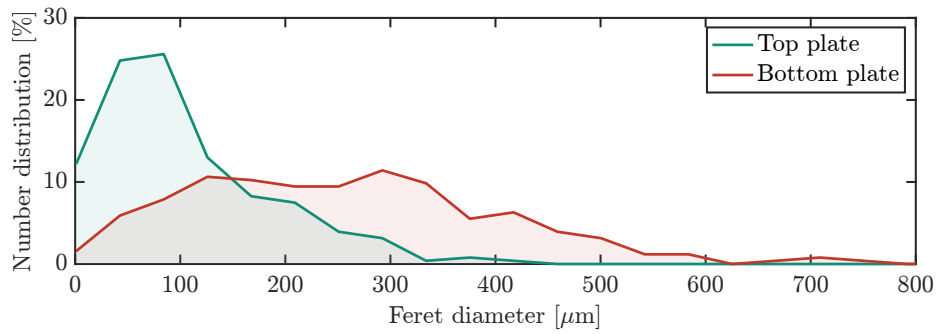


Figure 16: The number-based crystal size distribution of the crystals on the bottom (in red) and top plate (in green) shown in Figure 5 and 6 in the manuscript, respectively.

## 5 Shear stress response curves

Figures 17, 18, and 19 show shear stress response curves that were recorded during the nucleation experiments for various cases.

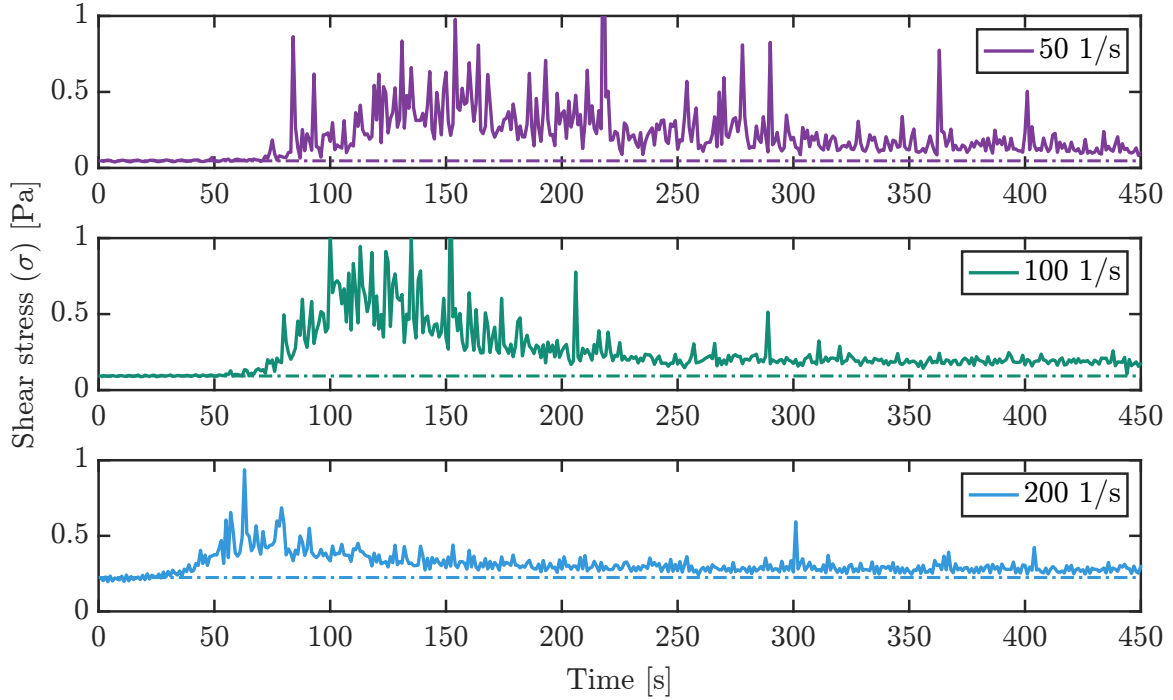


Figure 17: Shear stress ( $\sigma$ ) response curves for experiments conducted with global shear rates ( $\dot{\gamma}$ ) of 50, 100, and 200 1/s for a gap of 0.50 mm. The dash-dotted lines show the mean shear stress without nucleation for both cases. Strings were detected in all three experiments.

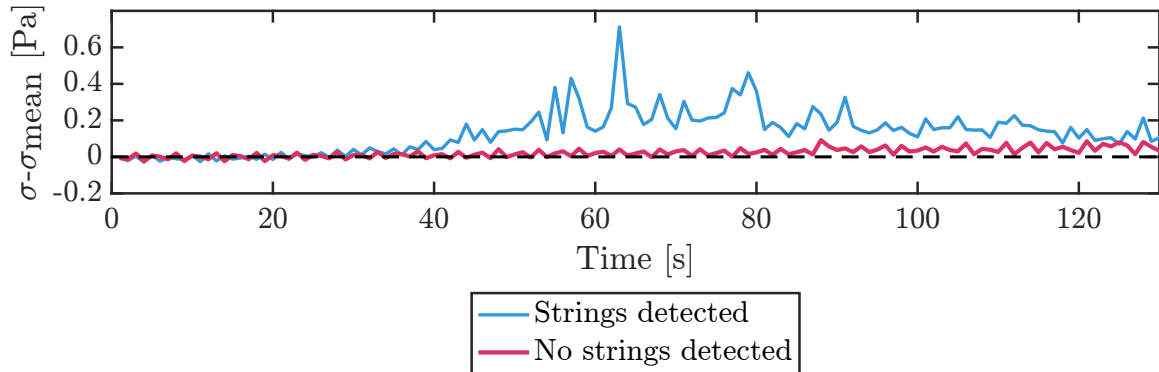


Figure 18: Shear stress ( $\sigma$ ) response curves for experiments conducted with a global shear rate of ( $\dot{\gamma} = 200$  1/s) and a gap of 0.50 mm with and without string formation. The mean shear stress is subtracted from the shear stress. The dashed black line is  $y = 0$ .

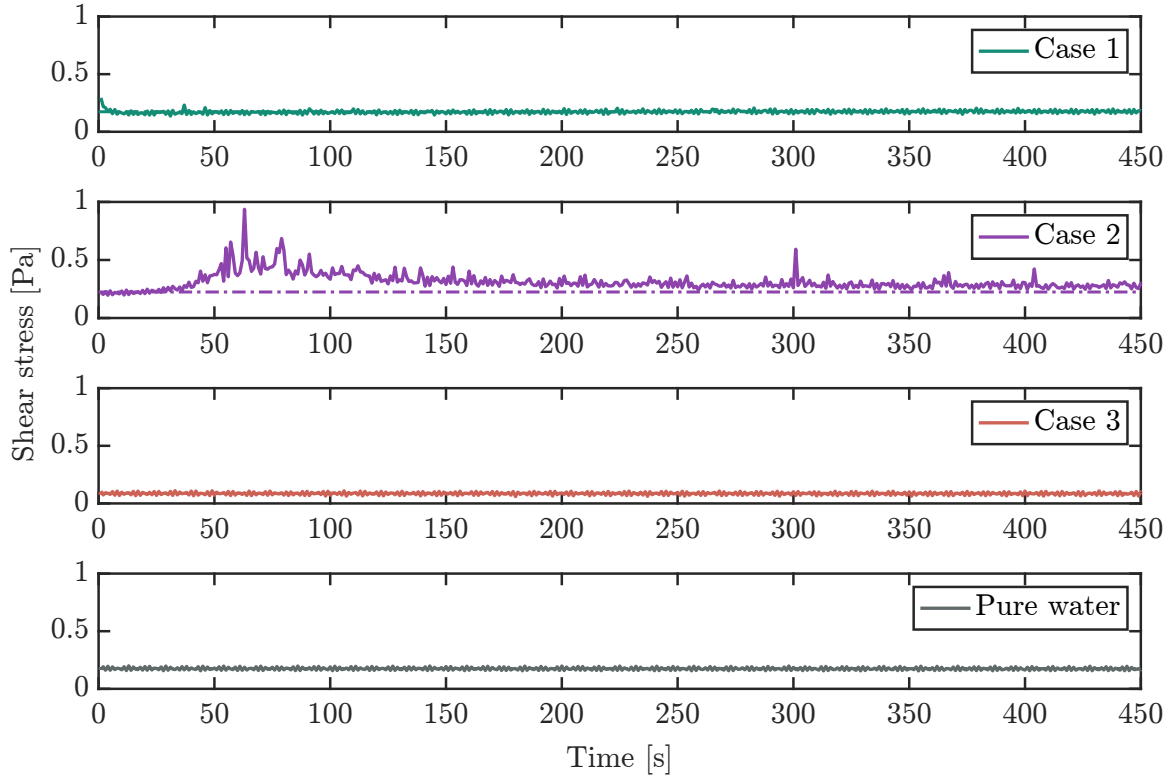


Figure 19: Shear stress ( $\sigma$ ) response curves for experiments conducted with a global shear rate of ( $\dot{\gamma} = 50$  1/s) and a gap of 0.50 mm. Case 1 (in green) shows an experiment where crystals were already present prior to crystallization. Case 2 (in purple) shows an experiment where crystals and a large amount of strings appear after shearing. Case 3 (in red) shows an experiment with a saturated concentration of PCM in water (thus a lower concentration compared to Case 1 and Case 2). The final curve shows the shear stress response curve for pure solvent (water). The dash-dotted lines show the mean shear stress without nucleation for both cases.

## 6 Video files

Four video files (SI.Video1.mp4, SI.Video2.mp4, SI.Video3.mp4, and SI.Video4.mp4) are included in the Supporting Information. The experiments shown in these video files were selected randomly.

The first three files show recordings of primary nucleation experiments performed in the parallel plate for various experimental conditions. The experimental conditions are always shown in the bottom right corner. In the first video (SI.Video1.mp4), the nucleation in circular patterns is shown. In the experiments shown in videos SI.Video2.mp4 and SI.Video3.mp4 there is no significant string formation. These videos also show that new crystals first appear at the edge of the plate (i.e. the zones with high local shear rates) and that the effect of centrifugal forces on the location of the crystals is negligible.

SI.Video4.mp4 shows the location at which crystals are detected (where every dot represents one crystal) for various experiments. The experimental conditions are shown in the bottom left

corner. The detected crystals are plotted on a dimensionless polar coordinate plot at the exact location at which they were detected. Each video shows the first 1000 crystals that are detected. The dimensionless radius ( $\tau$ ) is calculated using equation 4, such that  $\tau$  is 0 at the center of the plate (low local shear rate) and 1 at the edge of the plate (high local shear rate).

$$\tau = \frac{r}{R} \tag{4}$$